I R A M P
3(2), Dec. 2012, pp. 137-151

ISSN: 2229-3159

Analysis of Emission Spectra of Aluminum Monoxide in a Solid Propellant Flame

DAVID M. SURMICK[1], CHRISTIAN G. PARIGGER[1,A], ALEXANDER C. WOODS[1], A. B. DONALDSON[2], JONATHAN L. HEIGHT[2] AND W. GILL[3]

[1]University of Tennessee Space Institute, Center for Laser Applications, Tullahoma, TN 37388, USA
[2]New Mexico State University, Las Cruces, NM 88001, USA
[3]Sandia National Laboratories, Albuquerque, N87123, USA
Corresponding Author: E-mail: cparigge@tennessee.edu

ABSTRACT: The temperatures of regions in an aluminized solid propellant flame are determined as a function of height above the propellant surface from aluminum monoxide (AlO) and thermal emissions. Spectra from the solid propellant flames were fit using two models: AlO molecular emissions were fit with accurate line strength files while thermal emissions were fit for different emissivities. A Nelder-Mead algorithm is applied to infer temperature from diatomic AlO and thermal flame spectra. Thermal emissions are analyzed using the Planck's radiation law, and Wien's displacement law is derived for $1/\lambda$ and $1/\lambda^2$ wavelength dependent emissivity. Temperatures are obtained by linear least-square fitting to the measured spectra.

PACS numbers: 33.20.-t, 82.33.Vx,44.40+a.

Keywords: Molecular Spectroscopy, Flame and Combustion Diagnostics, Blackbody Radiation.

1. INTRODUCTION

Combustion of aluminum microparticles has various applications in materials that have high energetic releases. Such uses include applications in explosives [1, 2] and rocket motor propellants [3, 4]. Aluminum particles are added to these combustions because of its reduced activation energy, which is further reduced in the microparticle state. Due to this effect, aluminum microparticles are often added to these materials to increase the energy to the burns of these materials. The primary objective of this study is investigate the conditions that a payload attached to a rocket using solid propellant fuel sources might be subjected to under an accident scenario, such as an aborted take off. Under such a scenario, burning aluminum particles may impact surfaces of the rocket carrying sensitive payloads or nuclear power sources for payloads. The desire is to ensure the safety of sensitive materials in an aborted launch scenario.

Specifically, this work is aimed at accurately determining the temperature of the flame from the combusting solid propellant. Though the aluminum particles combust in a predictable manner, the role they play in an uncontrolled burn situation is not well understood. In such an accident scenario it is possible for the burning aluminum particles to impact and stick to surfaces, thus it is important to understand all the characteristics of aluminum particle combustion [5, 6, 7, 8, 9]. Accurately determining the temperature of the solid propellant flame is an important aspect of developing models of aluminum microparticle combustion [10, 11] and how they will effect the surfaces they impact during the combustion process.

Several temperatures are observed from a solid propellant plume and may indicate different combustion processes, such as alumina (Al_2O_3) vs. burning aluminum particles. Temperatures in this work are determined by analyzing spectral data from the solid propellant flames for aluminum monoxide (AlO) emissions and analyzing thermal emissions from the flame with thermal models that use constant and non-constant emissivities. The

stages of aluminum particle combustion are easily seen in the spectra of the burning aluminum, with one of the early stages being AlO which appears brightly in the spectra. Inferences on the temperature may be made by studying the spectra of AlO particles within the solid propellant flame, as the intensity of the diatomic AlO spectra is temperature dependent. Temperatures are determined by fitting the experimentally collected spectra to theoretical line strength files [12, 13] from the rotational and vibrational structure of the $B^2\Sigma^+ \rightarrow X^2\Sigma^+$ transition of the AlO spectra. Temperatures from the flame are also inferred from Planck law fitting to thermal emissions for particles with constant and wavelength dependent emissivities. To perform this analysis an assumption must first be made on the emissivity of particles in the flame. In this work, $1/\lambda$ and $1/\lambda^2$ wavelength dependent emissivities are investigated [14], as well as constant emissivity which corresponds to black-body radiators.

2. EXPERIMENTAL DETAILS

To determine the temperature of the flame as a function of height above the propellant surface, measurements were made along the height of the solid propellant plume via a vertical track [15]. The solid propellant used for this study was aluminized ammonia perchlorate. Spectral data were collected along the height of the vertical track using two Ocean Optics HR2000+ spectrometers. One had narrowband sensitivity in the range of 420-560 nm with a spectral resolution of 0.5 nm (SN HR+ C0979) and was used primarily to measure AlO emissions from the propellant flame. The other spectrometer (SN HR+ C0055) was sensitive in the broadband range of 200-1100 nm with a spectral resolution of 1.25 nm and was used primarily to record thermal emissions from the propellant flame. Further, the experiments were performed in 6.6 by 6.6 meter chamber that was vented from the bottom to purge smoke from the chamber. The chamber was at ambient conditions, analogous to the conditions of an controlled burn from a solid propellant source; i.e., atmospheric pressure and temperature. The equipment moved up and down the track through the use of a stepper motor that traveled at a rate of 0.014 m/s with data being collected once every second. The vertical track was 2.4 meters in height and 1.2 meters from the combusting solid propellant. Spectra from the interior regions of the flame were viewed through steel tubes with a ThorLabs RC12SMA-P01 collimating lens that was attached to the end of the tubing. The spectrometers were fiber optically coupled to the lens using an Ocean Optics QBIF 400 UV-VIS bifurcated fiber optic cable. The end of the steel tube was inserted into the flame and moved horizontally through the flame in increasing 25.4 mm (1 in.) steps up to 158 mm (6 in.). Horizontal measurements were recorded for flame heights of 152 mm (6 in.), 305 mm (12 in.), 508 mm (20 in.) which resulted in a data set of 18 spectrometer measurements for each of the broadband and narrowband spectrometers. The experimental procedure was repeated as well, giving an additional data set for each of the broadband and narrowband spectral data.

3. RESULTS

Spectral data was analyzed using the following steps: (1) the collected spectra were plotted for visualization purposes, (2) corrected for detector background and calibrated for detector sensitivity, (3) analyzed AlO spectra to determine the temperature as a function of height above the solid propellant plume, and (4) analyzed thermal emissions for constant and non-constant emissivity to infer temperature. Though each spectrometer had a targeted use, data for each spectrometer was used for both Planck law fitting and diatomic molecular AlO fitting. Figure 1 shows the calibrated data used to perform the temperature analysis in this work.

AlO spectra collected from the solid propellant flame were fit to known AlO line strength files using a Nelder Mead algorithm. The Nelder Mead algorithm is used for its ability to incorporate multiple variables, such as the spectral resolution of the equipment, and allows them to be fit simultaneously to spectra. To determine the temperature from a specific spectrometer arrangement, only the temperature was allowed to vary during fitting. The Nelder Mead algorithm is also used because it includes options for constant, linear, and quadratic baseline offsets, which enables fitting to occur even when background contributions are not well known. Figure 2 shows the fitting results for broadband and narrowband spectra and Table 1 shows the temperature fitting results for both narrow and broadband spectrometer data. Data having low signal to noise ratio has been omitted.

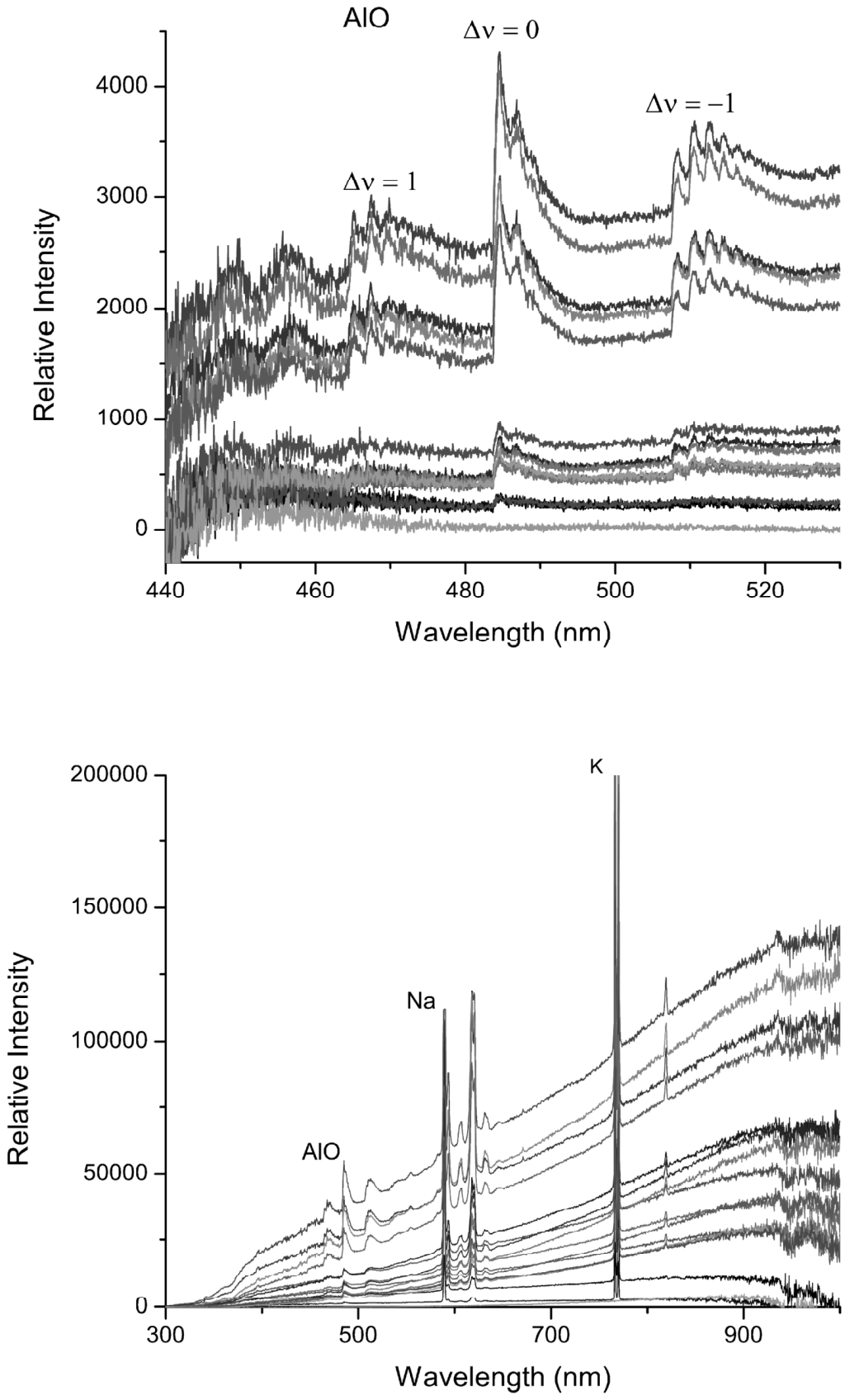

Figure 1: Calibrated data for Narrowband (top) and Broadband spectra (bottom)

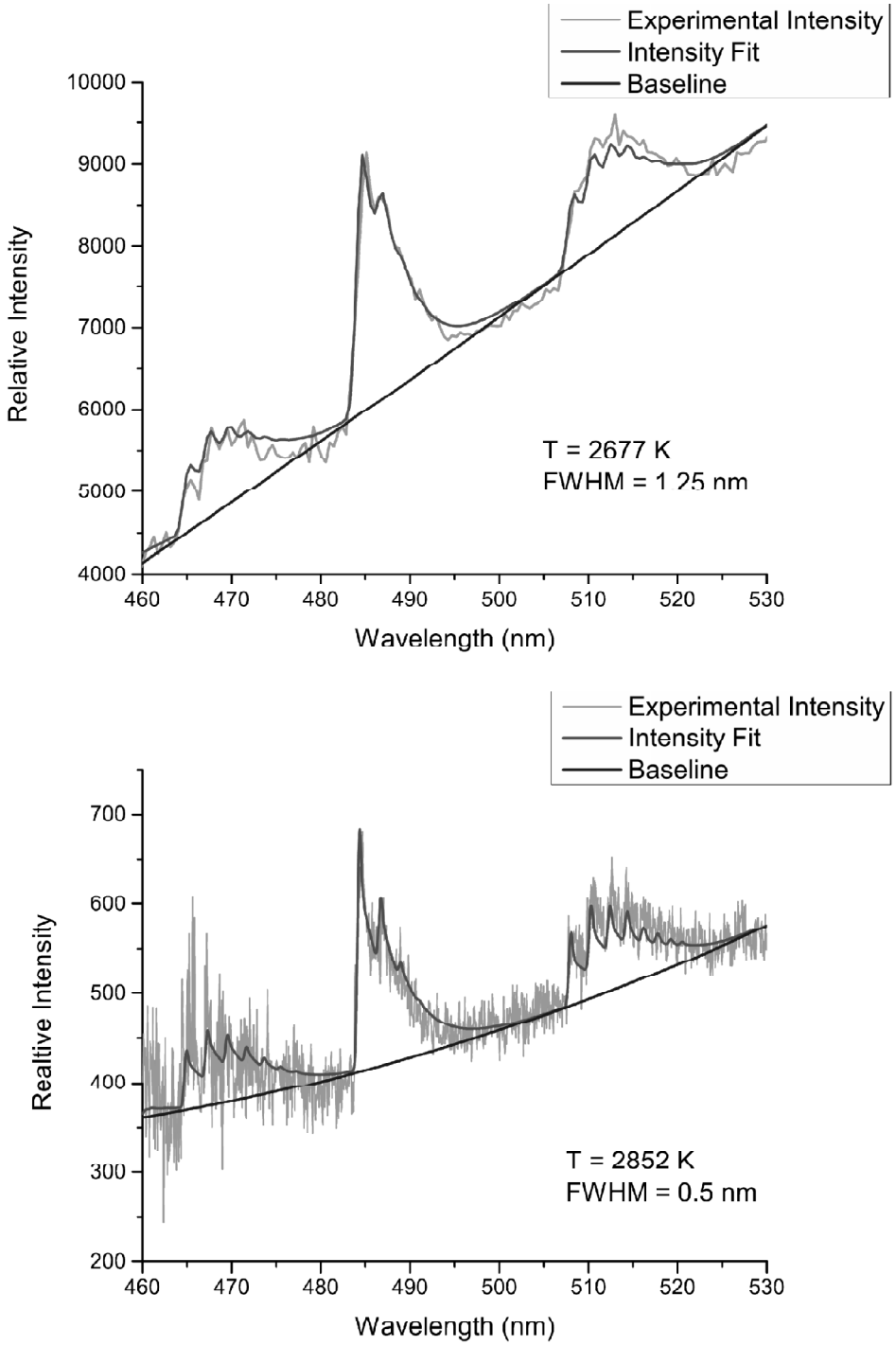

Figure 2: AlO fitting results for broadband (top) and narrowband (bottom) spectral data, including experimental fit, theoretical fit, and the baseline offset. Data corresponds to runs 15 and 17, respectively, for broadband and narrowband spectral data

The background thermal emissions from the recorded solid propellant flames are expected to be characterized by either black-body radiation models or thermal emission models with non-constant emissivities. Black-body radiation is characterized as having constant emissivity, $\varepsilon = 1$, while non-constant emissions are characterized as having wavelength dependent emissivities, $\varepsilon = \varepsilon(\lambda)$. In a recent of study of black-body radiation functions [16], Wien's displacement law is derived through use of poly-logarithms and is shown to be written as

Table 1
Inferred AlO temperature. Runs 1-12, 13-24, and 25-36 were collected at flame heights of 152 mm, 305 mm, and 508 mm, respectively. The temperature superscripts a, b, and c indicate the emissivity model of $\varepsilon = 1, 1/\lambda, 1/\lambda^2$, respectively, that yielded a temperature closest to the inferred AlO temperature. Data with low signal to noise ratio has been omitted (—)

		Temperature (K)	
Run	*Flame Depth (mm)*	*Narrowband*	*Broadband*
1	25	—	2845^b
2	51	—	2612^b
3	76	—	2767^b
4	102	—	2734^a
5	127	—	2626^b
6	152	—	—
7	25	—	2601^b
8	51	—	2461^b
9	76	—	2327^b
10	102	—	2384^b
11	127	—	2486^b
12	152	—	—
13	25	2958^c	2828^a
14	51	2998^c	2818^a
15	76	3064^b	2677^b
16	102	3010^a	2914^a
17	127	2852^c	2795^a
18	152	—	2768^a
19	25	2933^c	2743^a
20	51	2976^b	2740^a
21	76	3085^a	2837^a
22	102	3059^a	2739^a
23	127	—	2688^a
24	152	—	2767^a
25	25	3016^b	3139^a
26	51	2983^b	2980^a
27	76	2940*b*	2850^a
28	102	2873^c	2985^a
29	127	—	2713^a
30	—	—	
31	25	3037^b	2871^a
32	51	3061^b	2889^a
33	76	2991^a	2890^a
34	102	2875^a	2809^a
35	127	2788^c	2752^a
36	152	—	—

$$\lambda_{max,BB} \times T_{BB} = \frac{hc}{k_B} \frac{1}{5 + W_0(-5\exp^{-5})}$$
$$= 2.898 \times 10^6\, nmK, \quad (1)$$

where λ_{max} indicates the wavelength of the maximum spectral emission, T is the temperature of the black-body radiator, h is Planck's constant, c is the speed of light, k_B is Boltzmann's constant, and W_0 is the Lambert function. For sufficiently small arguments, the Lambert function may be approximated as $W_o(x) = x$, for $x = 1$, and the absence of the W_o term corresponds with the Wien approximation. Temperatures from a source with non-constant emissions can be determined from a modified Wien's displacement law. For $\varepsilon(\lambda) = 1/\lambda$ one finds

$$\lambda_{max,1/\lambda} \times T_{1/\lambda} = \frac{hc}{k_B} \frac{1}{6 + W_0(-6\exp^{-6})}$$

$$= 2.415 \times 10^6 \, nmK \tag{2}$$

and for $\varepsilon(\lambda) = 1/\lambda^2$

$$\lambda_{max,1/\lambda^2} \times T_{1/\lambda^2} = \frac{hc}{k_B} \frac{1}{7 + W_0(-7\exp^{-7})}$$

$$= 2.070 \times 10^6 \, nmK \tag{3}$$

One can see that the emissivities of $1/\lambda$ and $1/\lambda^2$ corresponds to a 5/6 and 5/7 reduction in the temperature-wavelength product, respectively, and leads to a modified Wien's displacement law. Particles within the flame that have non-constant emissivities will therefore show a temperature lowering effect [17, 18] as compared to black-body radiators. Figure 3 illustrates this effect for constant, $1/\lambda$, and $1/\lambda^2$ emissivities.

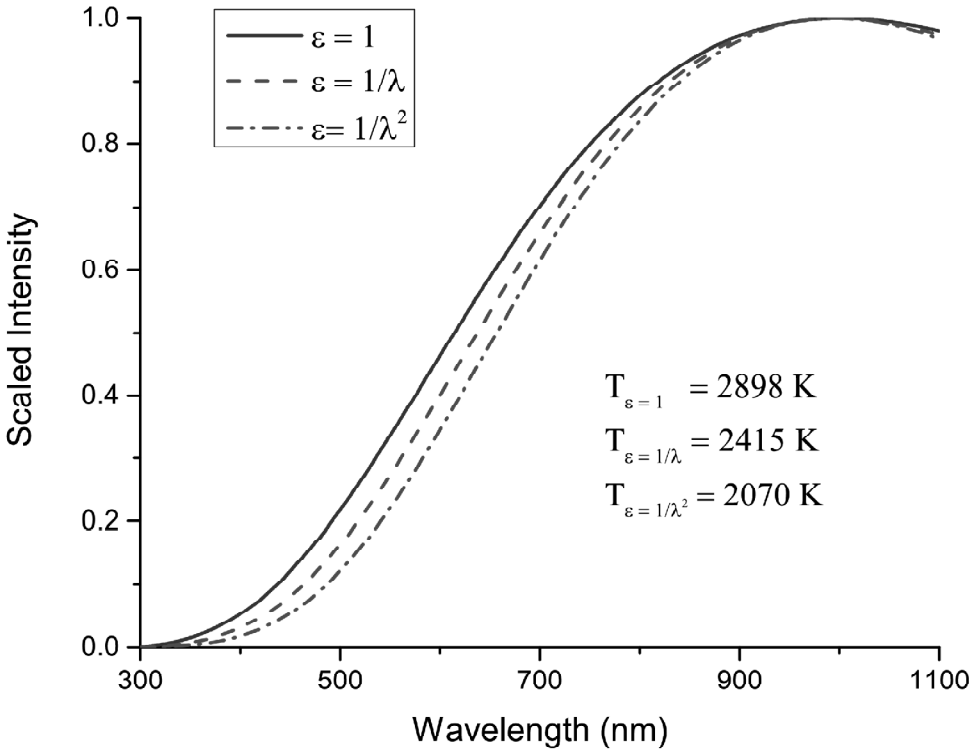

Figure 3: Wien's displacement law for constant, $1/\lambda$, and $1/\lambda^2$ emissivities with a peak wavelength set at 1000 nm

If one were to make an inference on the emissivity of the particles within flame from the combusting solid propellant, the temperature of the flame may be accurately determined through comparison to the temperatures found from AlO molecular fitting [17, 18, 19, 20, 21]. Planck's radiation law is used to analyze thermal emissions of the collected spectra. Maxima in our measured spectra occur near 950 to 1050 nm; however, our detector-

sensitivity is noticeably low near 1000 nm. Therefore, rather than direct application of Wien's displacement laws for constant, $1/\lambda$, and $1/\lambda^2$ emissivities, we directly apply Planck's radiation law as discussed below. In our analysis Planck's law may be expressed as

$$\ln\{C\ \frac{i_{\lambda,T}\cdot\lambda^5}{\varepsilon(\lambda,T)}\} = -\ln\{\exp[\frac{hc}{k_B}\ \frac{1}{\lambda T}]-1\}$$

$$\cong -\frac{hc}{k_B}\ \frac{1}{\lambda T}, \tag{4}$$

where $i_{\lambda,T}$ is the recorded spectral data, $\varepsilon(\lambda, T)$ is the emissivity, C is a constant, and T is the temperature of the radiating body. Equation 4 allows for straight line fitting to the data multiplied by λ^5 for black-body radiation, λ^6 for $\varepsilon = 1/\lambda$, and λ^7 for $\varepsilon = 1/\lambda^2$. The approximation from Equation 4 is valid for the wavelength range 400 to 1000 nm and may be used for straight line fitting. The error introduced by the approximation in Equation 4 is on the order of 1% for a temperature of 3000 Kelvin. For the straight line fits, the wavelength dependent nature for the emissivities only affects the log-scale, and therefore no inferences may be on the wavelength dependence of the particles in the flame.

The temperature of constant and nonconstant emitters from the propellant flame are determined by fitting a straight line using linear least squares fitting and then solving for the temperature as given by the expression for Planck's law from Equation 4. Figures 4 and 5 show linear fits for all three of the investigated emissivity models for broadband and narrowband spectrometer data, respectively. To accurately determine the temperature only thermal emissions are fit. Therefore, prior to fitting, all spectral lines were removed from the data sets. For narrowband spectrometer data contributions due to the AlO vibrational spectra were removed and for broadband spectrometer data contributions due to sodium (Na), potassium, (K), aluminum, and AlO were removed prior to fitting. The temperature results of the thermal radiation fitting are collected in Tables 2 and 3. Temperature results for data showing low signal to noise ratio have been omitted.

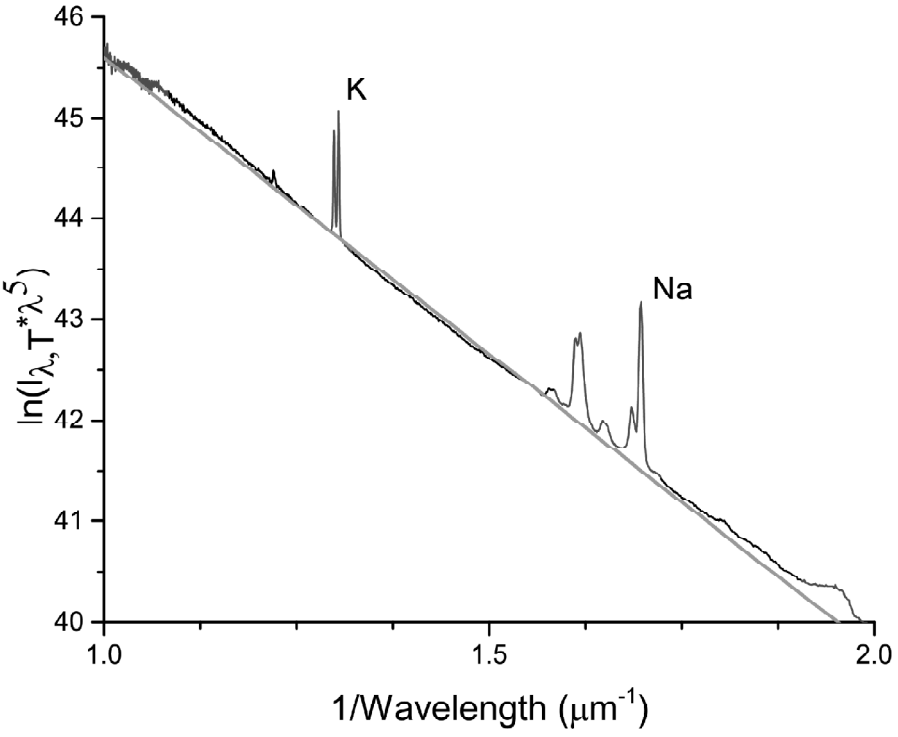

(a)

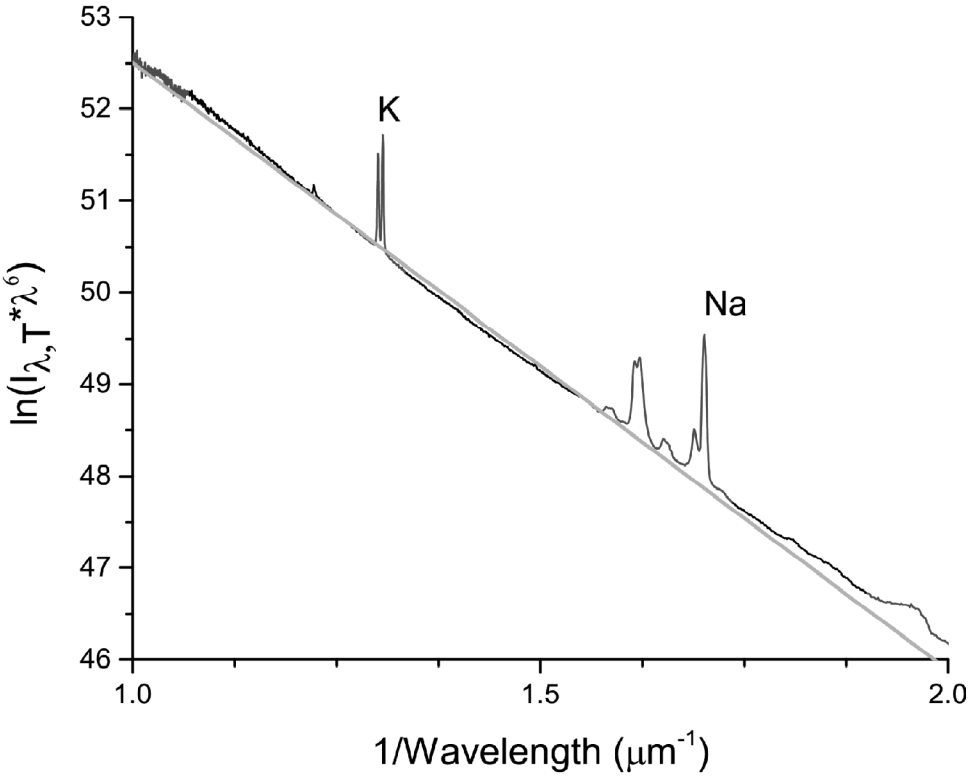

(b)

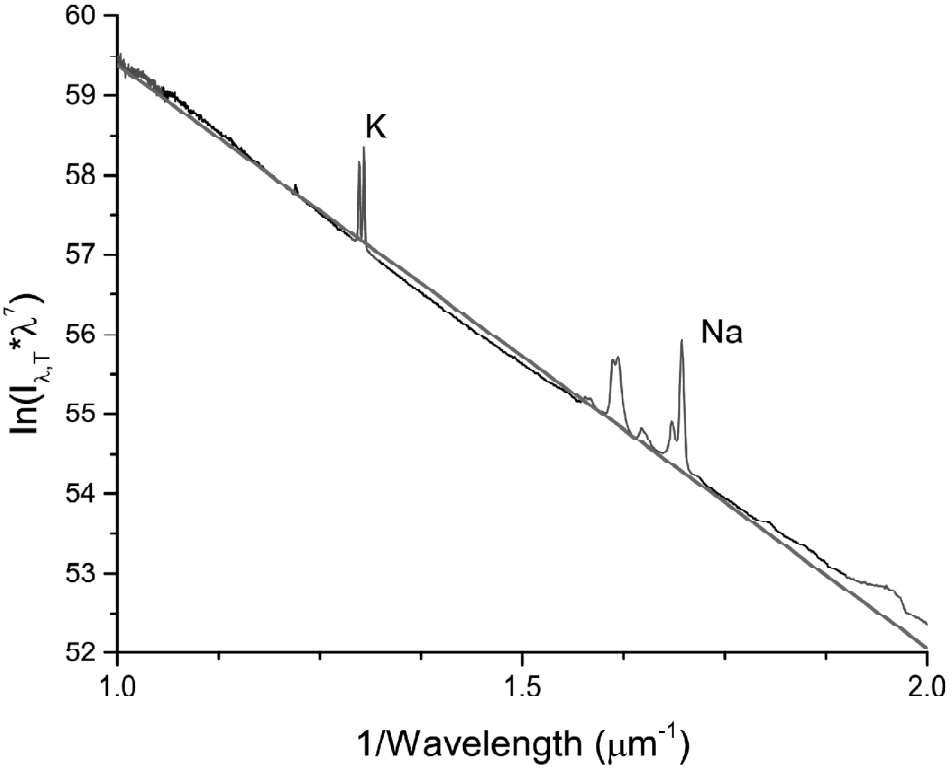

(c)

Figure 4: Broadband Planck law fitting for (a) black-body, (b) 1/λ and (c) 1/λ² thermal emission models. This data corresponds to run 15 from Table 2

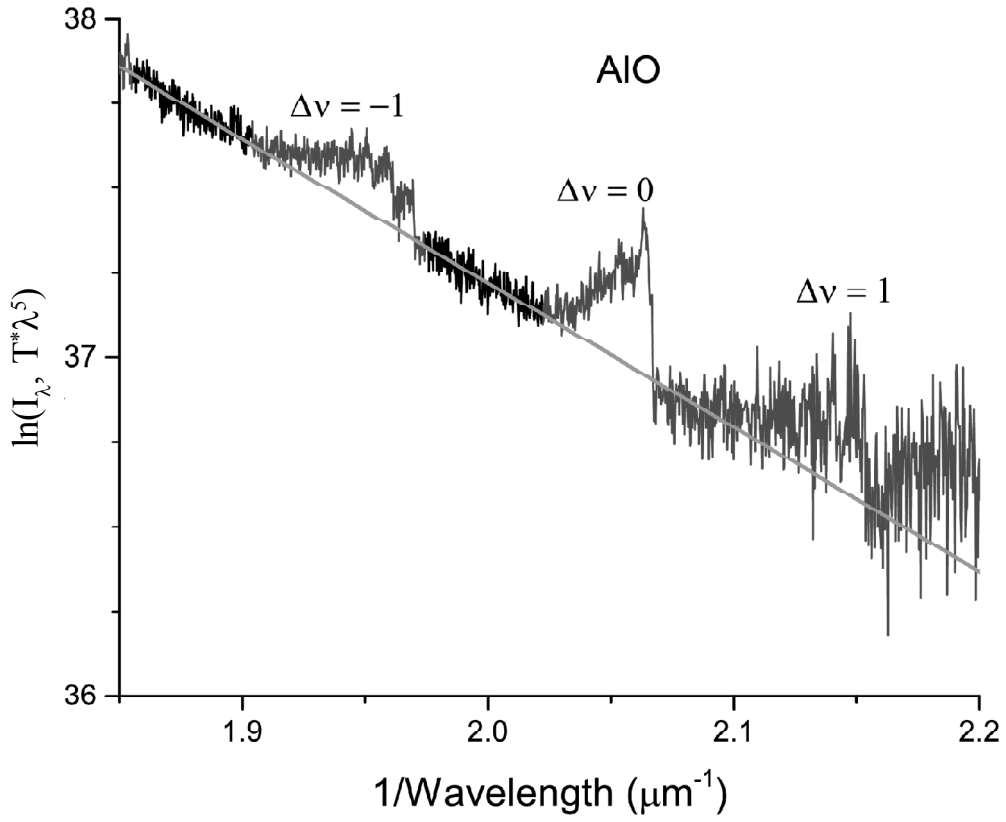
AlO
Δν = −1
Δν = 0
Δν = 1
ln(I_λ, T*λ^5)
38
37
36
1.9
2.0
2.1
2.2
1/Wavelength (μm^-1)

(a)

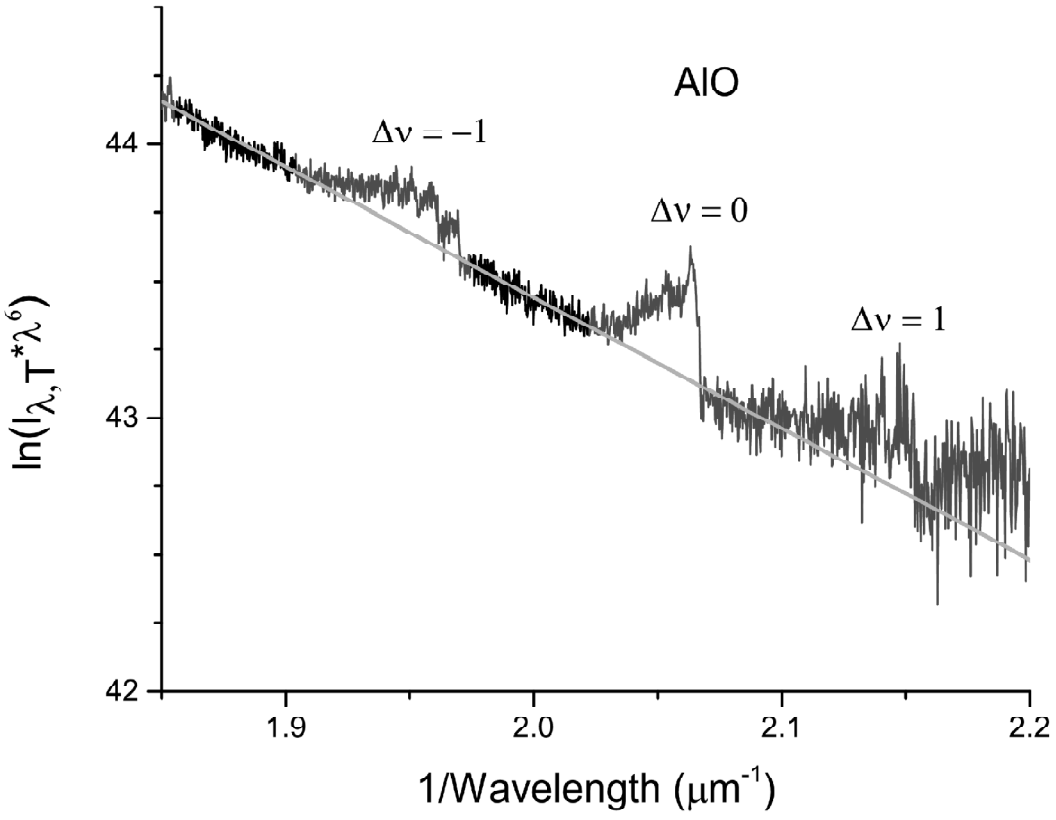
AlO
Δν = −1
Δν = 0
Δν = 1
ln(I_λ,T*λ^6)
44
43
42
1.9
2.0
2.1
2.2
1/Wavelength (μm^-1)

(b)

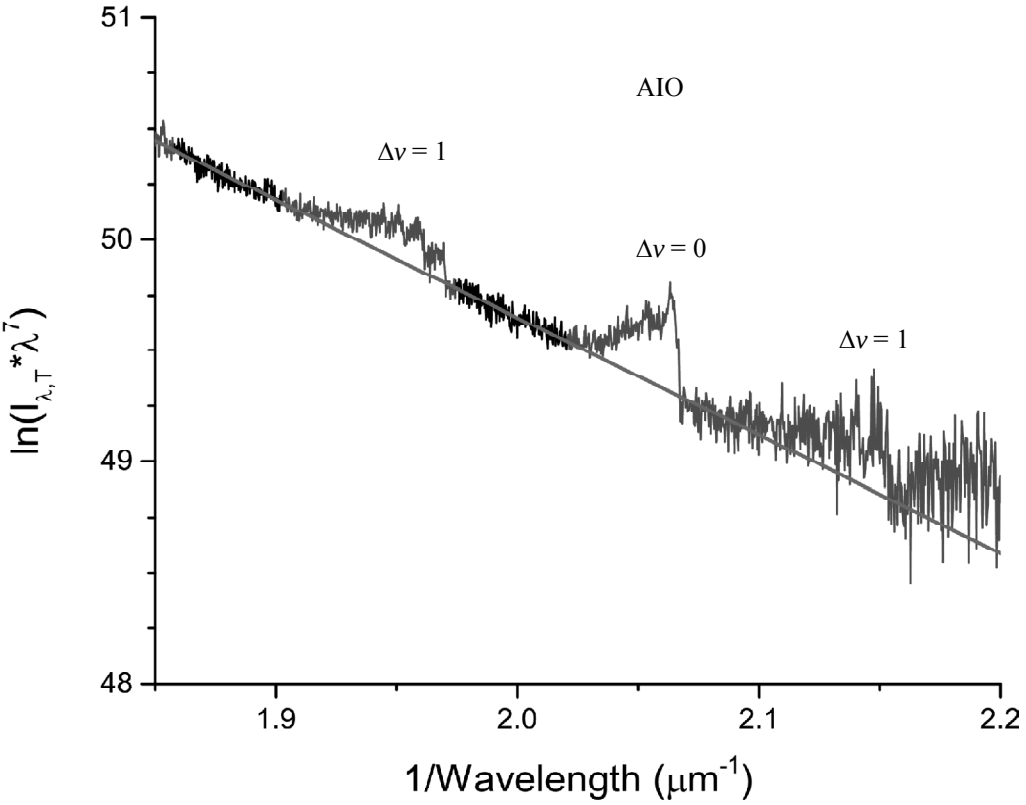

(c)

Figure 5: Narrowband Planck law fitting for (a) black-body, (b) 1/λ and (c) 1/λ² thermal emission models. This data corresponds to run 17 from Table 3

AlO molecular fitting of narrowband spectrometer data shows errors on the order of 2%. For a flame depth of 25 mm and height of 305 mm the temperatures are found to be 2958 Kelvin and 2828 Kelvin for narrowband and broadband spectrometer data, respectively (data run 13 from Table 1). For a similar flame depth at a flame height of 508 mm, the temperatures of narrowband and broadband spectrometer data are found to be 3016 Kelvin and 3139 Kelvin, respectively (data run 25). The differences in the determined temperatures are greater in the broadband data because the accuracy of the AlO fitting increases with increased spectral resolution. The resulting 1σ errors in the broadband data are on the order of 4%. Lower in the flame, temperatures are reported to be 2450 ± 100 Kelvin. Lower temperatures are seen in both the narrowband and broadband data.

Black-body radiation law, modified for constant and nonconstant emissivities, is applied to analyze thermal radiation from the flame versus wavelength. Least-square fitting is used for constant, 1/λ, and 1/λ² emissivities. These temperatures, as determined from the slopes of the narrowband and broadband data, are in general higher than those found for AlO molecular fitting. Using the indicated wavelength dependent emissivities leads to lower background radiation temperatures. Lower thermal radiation is also found for the center of the flame. This effect is demonstrated in Figure 6. The 1σ errors for temperatures obtained from Planck law fitting are determined to be on the order of 3%. For a flame depth of 102 mm and height 152 mm broadband data shows temperatures for constant, 1/λ, and 1/λ² emissivity are found to be 2754 K, 2419 K, and 2185 K, respectively (data set 4 from Table 2). The temperature found for 1/λ emissivity of 2445 K is in nice agreement with the AlO molecular temperature of 2419 K. Analysis of the narrowband data shows for a flame depth of 25 mm and height of 305 mm the Planck fitting temperatures are 3557 K, 3173 K, and 2846 K (data set 14 from Table 3). The result for 1/λ² emissivity is in nice agreement with the AlO molecular temperature of 2998 K. Results from the repeated experiments are consistent with each other, showing similar flame temperatures for similar flame depths as seen in Tables 2 and 3. Spectrometer data for each flame height is also plotted as a function of flame depth. These results show that there are lower

Table 2
Temperature results for broadband Plank law fittings. Runs 1-12, 13-24, and 25-36 were collected at flame heights of 152 mm, 305 mm, and 508 mm, respectively. Data with low signal to noise ratio has been omitted (—)

		Temperature (K)		
Run	*Flame Depth (mm)*	$\varepsilon = 1$	$\varepsilon = 1/\lambda$	$\varepsilon = 1/\lambda^2$
1	25	3181	2786	2500
2	51	2852	2512	2337
3	76	3269	2370	2144
4	102	2754	2419	2185
5	127	2837	2506	2238
6	152	—	—	—
7	25	2910	2745	2408
8	51	2813	2445	2204
9	76	2740	2403	2120
10	102	2758	2405	2163
11	127	2847	2455	2186
12	152	—	—	—
13	25	2888	2544	2264
14	51	2841	2561	2269
15	76	2444	2594	1920
16	102	2331	2107	1919
17	127	2414	2161	1967
18	152	2552	2169	2056
19	25	2790	2444	2180
20	51	2677	2398	2141
21	76	2230	2008	1835
22	102	2476	2214	1994
23	127	2552	2297	2060
24	152	2236	2006	1842
25	25	3311	2447	2192
26	51	2805	2401	2153
27	76	2741	2423	2193
28	102	2441	2220	1982
29	127	2600	2348	2106
30	152	—	—	—
31	25	2681	2293	2059
32	51	2497	2215	1989
33	76	2353	2116	1903
34	102	2323	2075	1871
35	127	2486	2209	1991
36	152	—	—	—

Table 3
Temperature results for narrowband Plank law fittings. Runs 1-12, 13-24, and 25-36 were collected at flame heights of 152 mm, 305 mm, and 508 mm, respectively. Data with low signal to noise ratio has been omitted (—)

		Temperature (K)		
Run	*Flame Depth (mm)*	$\varepsilon = 1$	$\varepsilon = 1/\lambda$	$\varepsilon = 1/\lambda^2$
1	25	—	—	—
2	51	—	—	—
3	76	—	—	—
4	102	—	—	—
5	127	—	—	—
6	152	—	—	—
7	25	—	—	—
8	51	—	—	—
9	76	—	—	—
10	102	—	—	—
11	127	—	—	—
12	152	—	—	—
13	25	6163	3209	2918
14	51	3552	3173	2846
15	76	2797	3063	2334
16	102	2922	2658	2418
17	127	3393	2556	2762
18	152	—	—	—
19	25	3580	3189	2893
20	51	3444	3092	2799
21	76	2689	2516	2304
22	102	3196	2816	2671
23	127	—	—	—
24	152	—	—	—
25	25	3483	3128	2812
26	51	3409	3094	2760
27	76	3511	3093	2755
28	102	5284	3073	27441
29	127	—	—	—
30	152	—	—	—
31	25	3319	3007	2741
32	51	3372	2993	2717
33	76	3003	2678	2534
34	102	3001	2747	2541
35	127	3294	2956	2672
36	152	—	—	—

temperatures in the central regions of the propellant flame, suggesting that there is greater oxidation at the edges of the plume. This also suggests that the flames are optically thick. The temperature profiles are plotted in Figure 6.

Flame temperatures are determined by comparing the AlO molecular fit temperatures with the temperatures determined from Planck law fitting with the three described emissivity models. Provided that the AlO emissions are in equilibrium with the thermal emissions, inferences may be made on the wavelength dependence of the emissivity. Higher in the flame, emissions are consistent with a $1/\lambda^2$ emissivity model. Lower in the flame, emissions are consistent with the $1/\lambda$ emissivity model.

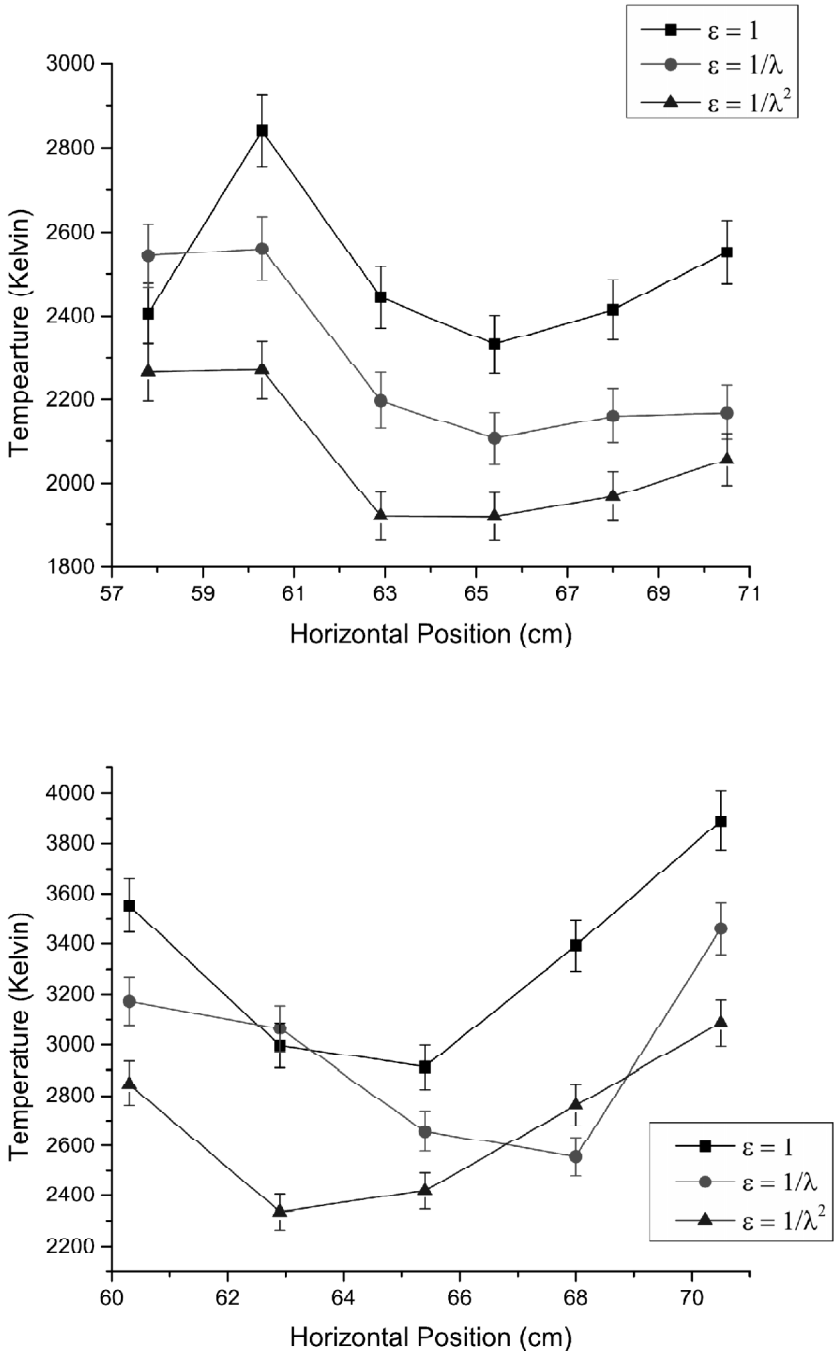

Figure 6: Temperature profiles for broadband (top) and narrowband temperature data for a flame height of 305 mm. The data plotted here corresponds to to runs 13-18 for both broadband and narrowband spectral data from Tables 2 and 3, respectively

4. DISCUSSION

Prior to temperature determination, the sensitivity of the spectral equipment must also be accounted for to accurately infer temperatures for both the AlO and thermal emissions. The effect of the calibration on temperature inferences for AlO molecular fits causes lower determined temperatures. Recent studies on aluminum containing nano-thermite reactions by Weismiller *et al.* [19] show similar results for temperature lowering to the current study when calibrating for equipment and background sensitivity. Related work by Goroshin *et al.* [18] finds higher temperatures of 3250 Kelvin when fitting various thermal radiation models to background emissions from an aluminum dust flame. The authors from Ref. [18] report temperature measurements to be within measurement accuracies from AlO emission spectra. Line-of-sight measurement of flames produced in air from this work and previously presented results [22, 23] show temperatures on the order of 2980 Kelvin in regions higher in the flame and 2450 Kelvin in regions lower in the flame, demonstrative of the temperature lowering effect mentioned above.

Studies of 100 μm aluminum droplets by Bucher *et al.* [24] and more recently by Gallier *et al.* [4] show a large gas phase temperature spread of 2350 Kelvin to nearly 4000 Kelvin near peak alumina (Al_2O_3) concentrations. Peak concentrations of AlO and Al_2O_3 are expected to occur for similar regions of the flame. Another study by Lynch *et al.* [21] showed a similarly large temperature range of 2500 Kelvin to 3500 Kelvin in determining the emissivity and temperature of combusting aluminum micro- and nanoparticles in high temperature particle clouds. Furthermore, the Aluminum combustion is not expected to be completed for heights of 1 meter above the combusting surface [25]. Measurements in this work focused on heights up to the order of 0.5 meters. Farther away from the surface, Al combustion temperature can be higher as for example communicated by Huang *et al.* [26]. However, velocity of burning particles can significantly affect combustion temperature in diffusion dominated regions [27] with reported temperatures less than 3000 K in laser-induced ignition following laser dispersion of metal fuel particles. Aluminum particles in that study are thought to be surrounded by a diffusion type flame.

5. CONCLUSION

The temperature of an aluminized solid propellant flame is determined as a function of height above the propellant surface. Flame temperatures were determined using non-linear fitting techniques on AlO emissions from the spectra of the flame and fitting thermal emissions of the flame using Planck's radiation law for constant and $1/\lambda$ and $1 / \lambda^2$ wavelength dependent emissivities. Comparison between the temperatures determined from the two techniques were used to make inferences about the radiation temperature from the propellant flame. AlO temperatures are lower than the those determined from the thermal emission analysis with the difference possibly arising from emissivities that are wavelength dependent. Results suggest that lower in the flame the emissivity is $1/\lambda$ wavelength dependent while higher in the flame the results suggest the wavelength dependence of the emissivity is $1/\lambda^2$. This corresponds with the observed trend of lower temperatures in regions higher in the flame, which is consistent with changes in temperature due to the wavelength dependency of the emissivity for differing regions of the propellant plume. Aluminum particles may be the cause of $1/\lambda^2$ wavelength dependent emissivity and bulk molten aluminum could result in $1/\lambda$ emissivity. Analysis of temperature profiles of the solid propellant flames indicates that there are lower temperatures in the central region of the flame. This implies that more oxidation occurs in the outer regions of the flame, in turn, suggesting that the solid propellant flame is optically thick.

Acknowledgements

This work is in part supported by Sandia National Laboratories, Purchase Order 1231736, and in part by the Center for Laser Applications at the University of Tennessee Space Institute. Sandia is a multiprogram laboratory operated by the Sandia Corporation, a Lockheed Martin Company, for the United States Department of Energy National Nuclear Security Administration under contract DEAC0494AL85000.

References

[1] J. R. Carney, J. S. Miller, and J. C. Gump, *Rev. Sci. Instr.* **77**, 063103, (2006), doi:10.1063/1.22007661.

[2] K. Benkiewicz and A. K. Hayashi, *AIAA Journal* **44**, 608-619, (2006).

[3] L. Meda, G. Marra, L. Galfetti, F. Severni, and L. De Luca, *Mater. Sci. Eng. C* **27**, 1993-1996, (2007).

[4] S. Gallier, F. Sibe, and O. Orlandi, *Proc. Comb. Inst.* **33**, 1949-1956, (2011).

[5] C. Badiola, R. J. Gill, and E. L. Dreizin, *Combust. Flame* **158**, 2064-2070, (2011).

[6] Z. X. Yan, J. Deng, and Z.M. Luo, *Mater. Charac.* **61**, 198-205, (2010).

[7] E. L. Dreizin, Combust. *Flame* **105**, 541-556, (1996).

[8] P. E. Bocanegra, D. Davidenko, V. Sarou-kanian, C. Chauveau, and I Göklap, Exp. Therm. *Fluid Sci.* **34**, 299-307, (2010).

[9] T. Bazyn, H. Krier, and N. Glumac, *Proc. Comb. Inst.* **31**, 2021-2028, (2007).

[10] G. Schloeffel, A. Eichhorn, H. Albers, Ch. Mundt, F. Seiler, and F. Zhang, Combust. Flame **157**, 446-454, (2010).

[11] N. I. Poletaev and A. V. Florko, Combut. Explo. Shock. **44**, 437-443, (2008).

[12] C. G. Parigger and J. O. Hornkohl, *Spectrochim. Acta, A* **81**, Issue 1, 404-411, (2011).

[13] I. G. Dors, C. Parigger, and J. W. L. Lewis, *Opt. Lett.* **23**, 1778-1780, (1998).

[14] C. F. Bohren and D. R. Huffman, *Absorption and Scattering of Light by Small Particles*, Wiley, New York, 1983.

[15] J. L. Height, B. Donaldson, W. Gill, and C.G. Parigger, Proceedings of IMECE2011, Denver, Colorado, USA, paper IMECE2011-62726, 2011.

[16] S. M. Stewart, J. Quant. Spectrosc. Radiat. *Transfer* **113**, 232-238, (2012).

[17] V. Tanguay, S. Goroshin, A.J. Higgins, and F. Zhang, *Combust. Sci. Tech.* **181**, 670-693, (2009).

[18] S. Goroshin, J. Mamen, A. Higgins, T. Bazyn, N. Glumac, and H. Krier, *Proc. Comb. Inst.* **31**, 2011-2019, (2007).

[19] M. R. Weismiller, J. G. Lee, and R. A. Yetter, *Proc. Comb. Inst.* **33**, 933-1940, (2011).

[20] M. Soo, P. Julien, S. Goroshin, J.M. Bergthorson, and D.L. Frost, Proc. Comb. Inst. (2012), http://dx.doi.org/10.1019/j.proci.2012.05.044.

[21] P. Lynch, H. Krier, and N. Glumac, *J. Thermophys. Heat Tr.* **24**, 301-308, (2010).

[22] C. G. Parigger, D. M. Surmick, A. C. Woods, A. B. Donaldson, J. Height, 8th US National Meeting of the Combustion Institute, Park City, UT, 2013.

[23] D. M. Surmick, A. C. Woods, and C. G. Parigger, Bull. APS, Vol. 57, paper KA 47 (2012).

[24] P. Bucher, R. A. Yetter, F. L. Dryer, T. P. Parr, and D. M. Hanson-Parr, Proc. Comb. Inst. **27**, 2421-2429, (1998).

[25] T. P. Parr and D. M. Hanson-Parr, Al Propellant Flame Structure, Private Communication, 2006.

[26] Y. Huang, G. A. Risha, V. Yang, and R. A. Yetter, Combust. *Flame* **156**, 5-13, (2009).

[27] A. A. Abdel-Hafez, M. W. Brodt, J. R. Carney, and J. M. Lightstone, *Rev. Sci. Intr.* **82**, 064101, (2011).